INORGANIC CHEMISTRY
FRONTIERS

RESEARCH ARTICLE

View Article Online
View Journal | View Issue

Cite this: *Inorg. Chem. Front.*, 2018, **5**, 2291

Lutetium(III) porphyrinoids as effective triplet photosensitizers for photon upconversion based on triplet–triplet annihilation (TTA)†

Zi-Shu Yang, Yingying Ning, Hao-Yan Yin and Jun-Long Zhang *

Received 23rd May 2018,
Accepted 4th July 2018

DOI: 10.1039/c8qi00477c

rsc.li/frontiers-inorganic

We described the first application of lanthanide complexes of porphyrinoids, exemplified by lutetium (Lu), as efficient photosensitizers in photon upconversion (UC) based on triplet–triplet annihilation (TTA). Compared to the widely used d block metals, Lu(III) porphyrinoids exhibit a better sensitization ability in photon UC based on TTA (TTA-UC), which is ascribed to the extra-long triplet lifetime compared with the d block metal counterparts, using 9,10-bis(2-phenylethynyl)anthracene (BPEA) or rubrene as an acceptor. Notably, the Lu(III) complex of the porphyrin (**Lu-1**)/BPEA pair showed a high upconversion efficiency of 12.4% in degassed toluene. Importantly, to demonstrate the potential application of Lu porphyrinates in TTA-UC based bioimaging, we prepared nanomicelles and mesoporous silica nanoparticles with **Lu-1**/BPEA or Lu(III) porpholactone (**Lu-2**)/BPEA pairs. In living cell imaging, the capability of **Lu-1** or **Lu-2** as a TTA-UC sensitizer has been observed, displaying their potential application in biological studies. This work enriches the repertoire of metal sensitizers in TTA-UC with the capability of living cell imaging and, more importantly, also extends the scope of lanthanide coordination chemistry to lanthanide chemical biology related to biological optical materials and medicine.

Introduction

Photon upconversion based on triplet–triplet annihilation (TTA-UC) has been attracting increasing attention for potential applications in solar cells, bioimaging, photodynamic therapy, and photocatalysis.[1–6] Since singlet–triplet intersystem crossing (ISC) is often forbidden in organic chromophores, incorporating heavy atoms (*e.g.*, transition metals) becomes a prevalent approach to enable spin-orbital coupling and generate a triplet excited state.[7,8] Thus the choice of metals is critical for the design of triplet photosensitizers. Extensive studies have been focused on transition metals such as Pd, Pt, Ir, Ru and Re due to their large spin–orbit coupling constants (ζ).[2,9,10] In sharp contrast to d-block metals, the usage of f-block metals including lanthanides (Lns) has seldom been reported. In principle, Lns have large ζs (556–2838 cm^{-1}) due to their large nuclear charges.[8] For example, lutetium (Lu) has a ζ of 1153 cm^{-1}, comparable to palladium (1504 cm^{-1}) and ruthenium (1042 cm^{-1}) but smaller than platinum (4481 cm^{-1}) and rhenium (2903 cm^{-1}).[8] Importantly, lanthanide coordination always leads to effective ISC process, allowing energy transfer from the lowest triplet state of a chromophore to the excited states of Lns.[11,12] More importantly, Gd(III) and Lu(III) complexes, especially with porphyrinate ligands, exhibit a strong ligand-centered phosphorescence with long lifetimes up to milliseconds due to the closed shell electronic structure of Lu(III) (f^{14}) or the high-lying f–f transition of the Gd(III) ion.[13] Thus, these features make Ln complexes good triplet sensitizer candidates not only in O_2 sensing, photodynamic therapy (PDT), and photocatalysis[14] but also in potential photon upconversion based on TTA.

Porphyrinoids are important chromophore ligands for constructing metal sensitizers due to their good coordination ability, strong absorption from the visible to near-infrared (NIR) region, and tunable triplet states by β- or meso-modification.[15] Because of our continued interest in porpholactones, in which one or two pyrroles in porphyrin are replaced by an azlactone moiety,[16,17] we and others applied Gd(III) porphyrinoids including porpholactone and *cis*/*trans*-porphodilactones as photosensitizers in O_2 sensing, PDT and photocatalysis.[18–20] Since the Gd(III) ion has seven unpaired electrons (f^7), which was found to quench the phosphorescence with a shorter lifetime than the diamagnetic Lu(III) counterpart due to the paramagnetic metal effect,[21,22] we

Beijing National Laboratory for Molecular Sciences, State Key Laboratory of Rare Earth Materials Chemistry and Applications, College of Chemistry and Molecular Engineering, Peking University, Beijing 100871, P. R. China.
E-mail: zhangjunlong@pku.edu.cn; Fax: +86-10-62767034

† Electronic supplementary information (ESI) available: Detailed characterization and photophysical data. See DOI: 10.1039/C8QI00477C

herein report a proof-of-concept study using Lu porphyrinoids as the triplet photosensitizers for TTA-UC.

Based on our previously reported lanthanide porphyrinoids,[19,20,23–27] we synthesized Lu(III) complexes of tetrapentafluorophenylporphyrin (**Lu-1**), porpholactone (**Lu-2**) and *cis*/*trans*-porphodilactone (**Lu-3**/**4**), using the Kläui tripodal ligand $[(\eta^5\text{-}C_5H_5)Co\{(OMe)_2P{=}O\}_3]$ (L_{OMe})[28] as an auxiliary axial ligand. Following a systematic examination of their sensitization efficiency in TTA upconversion, we found a higher upconversion quantum yield of **Lu-1** than **Gd-1**, **Pd-1**, and **Zn-1** with the same porphyrin ligand, using 9,10-bis(2-phenylethynyl)anthracene (BPEA) as the acceptor. Moreover, to demonstrate the potential application of Lu(III) porphyrinates in biological studies, we demonstrated the capability of **Lu-1** or **Lu-2** as a TTA-UC sensitizer in living cell imaging experiments. To our knowledge, this work presents the first example of lanthanide coordination complexes as photosensitizers for TTA photon upconversion and provides an access to the further development of lanthanide chemical biology.

Results and discussion

Synthesis and characterization

Following the previously reported procedures,[29] we synthesized and characterized four Lu(III) complexes of tetrapentafluorophenylporphyrin (**Lu-1**), porpholactone (**Lu-2**) and *cis*/*trans*-porphodilactones (**Lu-3**/**4**) (Fig. 1a) starting from the corresponding free base. **Lu-1**/**2**/**3**/**4** were obtained in the yields of 82, 80, 76, and 69%, respectively. We also chose transition metal complexes **Pd-1** and **Zn-1**, and a Gd(III) analogue (**Gd-1**) as the controls. The detailed synthetic procedures and characterization by ^{1}H, ^{13}C, ^{19}F NMR and IR spectroscopy and HR ESI-mass spectrometry (Fig. S1–20†) are listed in the Experimental section and the ESI.†

Photophysical properties

The absorption and emission spectra of **Lu-1–4** were obtained in deaerated toluene (Fig. 1b and c) and the photophysical data are summarized in Table 1. As shown in Fig. 1b, **Lu-1–4**

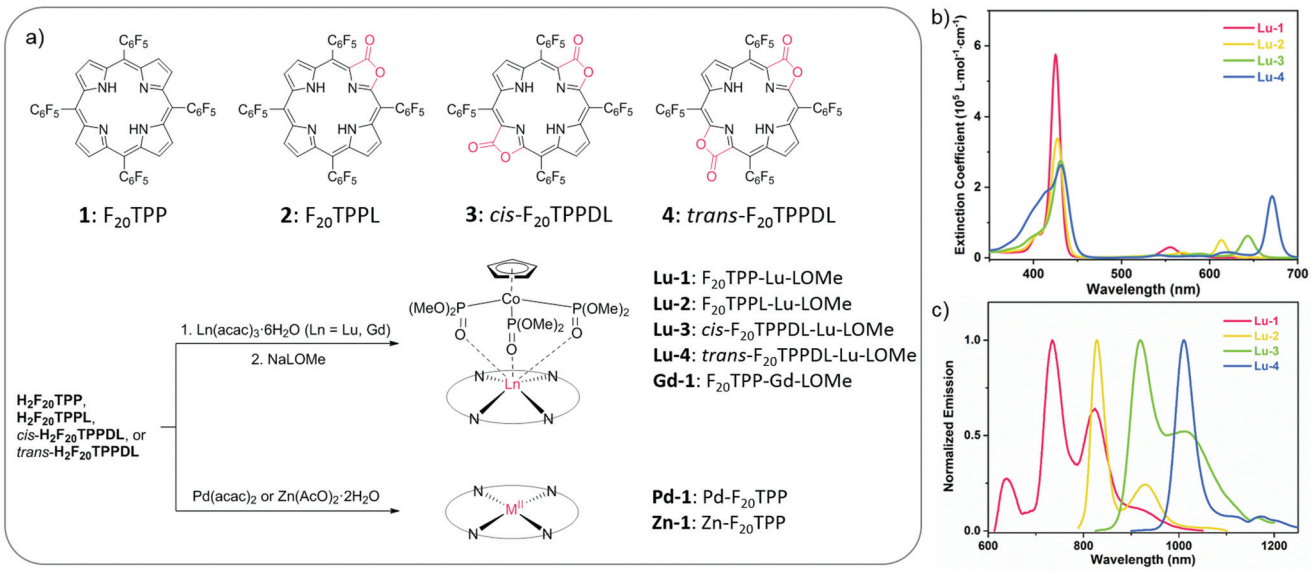

Fig. 1 (a) Structures and synthesis procedures of the triplet sensitizers in this work. (b) UV/Vis absorption and (c) normalized emission spectra (excited at 425 nm) of **Lu-1–4** in degassed toluene at room temperature.

Table 1 Absorption and emission properties of **Lu-1–4** and **M-1** (M = Gd, Pd, Zn)[a]

Compound	UV-Vis λ_{max}/nm (log ε/[M^{-1} cm^{-1}])	Luminescence λ_{max}/nm (τ_P/μs)	Φ_P [b] (%)
Lu-1	425(5.76), 554(4.39), 590(3.69)	734(2.4 × 10^3), 824	2.2
Lu-2	427(5.53), 568(3.61), 614(4.67)	827(549.2), 928	1.4
Lu-3	431(5.44), 541(3.84), 589(4.07), 643(4.60)	919(218.8), 1015	0.4
Lu-4	431(5.42), 535(3.93), 611(4.13), 670(5.15)	1010(262.6), 1115, 1172	0.1
Gd-1	425(5.61), 556(4.24), 590(3.53)	741(104.7), 834, 930	5.3[c]
Pd-1	411(5.22), 521(4.26), 554(4.18)	671(414.9), 702, 737	11[d]
Zn-1	421(5.48), 547(4.20), 580(3.64)	585, 641, 713(880.0)	0.8[e]

[a] Measured in degassed toluene at room temperature in this work unless noted otherwise. [b] Using ZnTPP in toluene (Φ = 3.3%)[30] as a reference. [c] Previously reported as 3.9% in degassed CH_2Cl_2 using ZnTPP in toluene (Φ = 3.3%) as a reference.[19]. [d] Previously reported as 0.11 in degassed toluene using $Ir(C_s)_2$(acac) in degassed $CHCl_3$ (Φ = 54%) as a reference.[31]. [e] In 3-methylpentane at 77 K, from ref. 32.

exhibit intense Soret bands centered at 420–430 nm and Q bands at *ca.* 500–700 nm. Compared with **Lu-1**, $Q_y(0,0)$ bands of **Lu-2–4** showed red-shifts of 18, 53 and 80 nm, respectively, and the extinction coefficients ($\log \varepsilon[M^{-1}\ cm^{-1}]$) increase from 3.69 to 4.67, 4.60 and 5.15, similar to the tendency of the previously reported Gd(III) series.[19] Upon irradiation at the Soret or Q band, **Lu-1–4** displayed intense NIR phosphorescence, which was completely quenched in air, with maxima at 734, 827, 919, and 1010 nm, respectively (Fig. 1c). Accordingly, the lowest triplet states (E_{T1}) of **Lu-1–4** were estimated to be 1.72, 1.54, 1.41 and 1.26 eV, respectively, in line with the trend of triplet state energy levels of **Gd-1–4**.[19] The mechanism that β-lactonization accelerates the radiative rate from porphyrin, porpholactone to *cis*/*trans*-porphodilactones is not clear at the current stage and we ascribed it to the hybridization of the n–π* transition in excited states arising from the C=O moiety. The decay curves were satisfactorily fitted by the mono-exponential function, giving the lifetimes of 2.4, 0.5, 0.2 and 0.2 ms for **Lu-1–4**, respectively. The quantum yields were respectively recorded as 2.2, 1.4, 0.4, and 0.1% using (5,10,15,20-tetraphenylporphyrinato)zinc(II) (ZnTPP, Φ = 3.3%, in toluene)[30] as a reference. The measured lifetimes and quantum yields decreased with the extent of β-modification, suggesting the effectiveness to modulate the triplet states of porphyrinoids by β-lactonization. As shown in Fig. S21b† and Table 1, **Gd-1** and **Pd-1** displayed phosphorescence, while **Zn-1** displayed fluorescence with a weak phosphorescence band at *ca.* 710–800 nm (at 77 K). Notably, **Lu-1** has the longest triplet lifetime (2.4 ms) among four metal complexes (**Gd-1**, 105 μs; **Pd-1**, 415 μs; **Zn-1**, 880 μs).

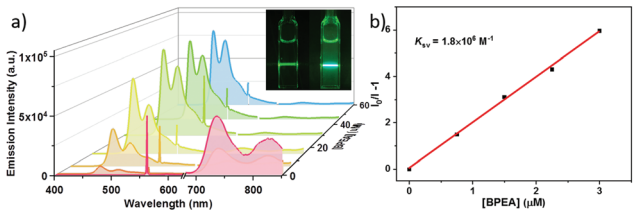

Fig. 2 (a) Luminescence spectra of **Lu-1** with BPEA at different concentrations. Inset presents the photographs of BPEA (left) and **Lu-1**/BPEA (right) solution irradiated with a 561 nm laser. (b) Stern–Volmer plot of **Lu-1** with BPEA ([**Lu-1**] = 0.5 μM, λ_{ex} = 561 nm, 480 mW cm^{-2}, in degassed toluene at room temperature).

Triplet–triplet annihilation upconversion

To examine the efficiency of Lu(III) porphyrinates in TTA-UC, we chose BPEA (E_T = 1.53 eV)[33] as the acceptor for **Lu-1** and **Lu-2**, and rubrene (E_T = 1.14 eV)[34] for **Lu-3** and **Lu-4**, making sure that E_Ts of acceptors are slightly lower than E_{T1}s of photosensitizers. As shown in Fig. 2a, the addition of BPEA to the degassed toluene solution of **Lu-1** (0.5 μM) gradually quenched the phosphorescence (excited at 561 nm, the Q band of **Lu-1**). The quenching constant (K_{sv}) of 1.8 × 10^6 M^{-1} was determined by Stern–Volmer plot analysis (Fig. 2b). When the concentration of BPEA reaches 60 μM, the phosphorescence of **Lu-1** was nearly quenched, giving the triplet–triplet energy transfer efficiency (Φ_{TTET}) of *ca.* 0.99.[32] Under identical conditions, **Gd-1**, **Pd-1**, and **Zn-1** displayed K_{sv}s as 1.2 × 10^5, 1.3 × 10^6, and 1.4 × 10^6 M^{-1}, respectively, with BPEA, and Φ_{TTET} as 0.84, 0.98, and 0.90 respectively (Fig. S22–24†). The results indicate that **Lu-1** has a higher K_{sv} and Φ_{TTET} than **Pd-1**, **Zn-1**, and **Gd-1** with the same porphyrin ligand.

As expected, excitation at 561 nm led to the anti-Stokes fluorescence maximum at *ca.* 480 nm (**Lu-1**/BPEA = 0.5/60 μM), which is the fluorescence from BPEA. It is worth noting that in the absence of **Lu-1**, no BPEA fluorescence was observed under the same conditions. As shown in Fig. 3, the double logarithmic plots of emission intensity as a function of incident power density showed a transition from quadratic dependency

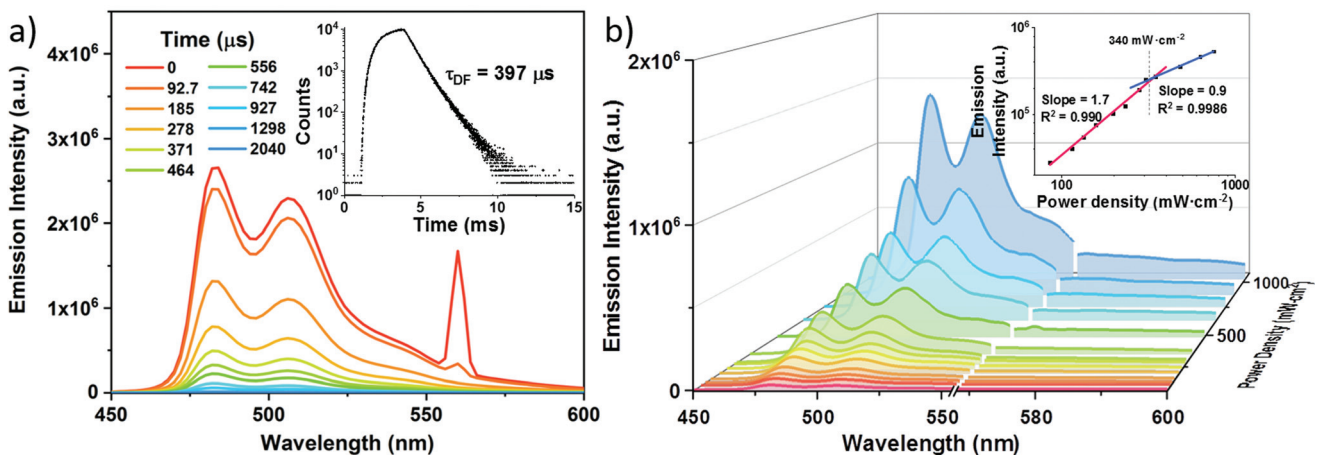

Fig. 3 (a) Time resolved emission spectra of the TTA upconversion system with **Lu-1**/BPEA. Inset presents the decay spectrum at 480 nm (τ_{DF} = 397 μs) measured on a Horiba Jobin Yvon DeltaFlex ultrafast lifetime spectrofluorometer. (b) Upconverted fluorescence spectra of **Lu-1**/BPEA at different excitation powers. Inset presents the double logarithmic plots of upconversion intensity at 480 nm measured as a function of the power density of the incident laser for **Lu-1**/BPEA solution (the threshold excitation power density = 340 mW cm^{-2}) ([**Lu-1**] = 0.5 μM, [BPEA] = 60 μM, λ_{ex} = 561 nm, in degassed toluene).

(slope = 2) in the low power density region (<340 mW cm^{-2}) to linear dependency (slope = 1) in the high power density region (340–1000 mW cm^{-2}). This is in accordance with the anti-Stokes emission generated by TTA-UC. To validate the TTA-UC luminescence, the fluorescence lifetime of 397 μs and the time resolved emission spectra (TRES) of the **Lu-1**/BPEA system were recorded (Fig. 3a), suggesting a delayed fluorescence due to TTA-UC. The upconversion efficiency (Φ_{UC}) increased along with the increasing BPEA concentration, and culminated in 12.4% at [BPEA] = 60 μM ([**Lu-1**] = 0.5 μM, Fig. S34†). In addition, the UC fluorescence decreased negligibly under irradiation at laser power = 480 mW cm^{-2} for more than 2 h (Fig. S35†), indicating the long-term stability. Similarly, **Gd-1**, **Pd-1**, and **Zn-1** were used as controls and Φ_{UC}s of 8.6, 6.3 and 1.3% were obtained respectively, lower than that of **Lu-1** (12.4%) (Fig. S28–30†).

Using **Lu-2–4** as photosensitizers and BPEA or rubrene (E_T = 1.14 eV) as the acceptors, which are dependent on the E_Ts of photosensitizers (Fig. S25–27 and S31–33†),[34] the K_{sv}s of 7.1×10^5, 7.0×10^4 and 4.6×10^4 M^{-1} were obtained in the **Lu-2**/BPEA, **Lu-3**/rubrene, and **Lu-4**/rubrene systems. Accordingly, Φ_{UC} of 7.8% in **Lu-2**/BPEA (0.5/60 μM) was lower than that of **Lu-1** but comparable to **Pd-1**. However, when **Lu-2** was used as the photosensitizer, the incident wavelength could be shifted above 600 nm due to the red-shifted Q band compared to that of **Lu-1**. **Lu-3** and **Lu-4**/rubrene pairs showed Φ_{UC}s of 0.9 and 0.5% ([**Lu-3**/**4**] = 0.5 μM, [rubrene] = 200 μM). Compared with previously reported Pd(II) and Pt(II) analogues,[36] **Lu-3**/**4** displayed a comparable sensitization ability for rubrene, even at a lower photosensitizer concentration of 0.5 μM. These results suggest that Lu(III) porphyrinoids exhibit a good sensitization ability in photon UC based on TTA, comparable to and even better than the widely used d block metals.

To understand the kinetics of **Lu-1** sensitizing photon upconversion, we used **Gd-1**, **Pd-1** and **Zn-1** to compare several photophysical parameters according to eqn (1). Φ_{UC} is the product of intersystem crossing efficiency (Φ_{ISC}) of the sensitizer, the triplet-triplet energy transfer efficiency (Φ_{TTET}) from the sensitizer to the acceptor, the TTA efficiency (Φ_{TTA}) of the acceptor, and the fluorescence quantum yield (Φ_F) of the acceptor. For Φ_F of BPEA is *ca.* 1.0 in toluene,[37] Φ_{UC} values are only affected by Φ_{ISC}, Φ_{TTET}, and Φ_{TTA}. Due to the lack of heavy atoms, Φ_{ISC} of **Zn-1** is relatively small and thus Φ_{UC} is the smallest. For the other compounds, Φ_{ISC} values are assumed to be near unity (1.0) due to a similar heavy atom effect.[7,38] Φ_{TTA}s for **Lu-1**, **Gd-1**, and **Pd-1** were then estimated using eqn (1) to be 12.5, 7.5 and 8.8%, respectively (Table 2). Generally, both TTET and TTA processes belong to bimolecular dynamic quenching and depend on diffusional interactions, thus longer triplet lifetimes of either sensitizers or acceptors benefit Φ_{UC}.[1] In this work, we observed the order of phosphorescence lifetimes for **Lu-1** (2.4 ms) > **Pd-1** (0.4 ms) > **Gd-1** (0.1 ms), which is consistent with the tendency of Φ_{TTET}, Φ_{TTA}, and Φ_{UC} for these complexes. Thus, we assumed that the long-lived triplet state of **Lu-1** might be ascribed to a higher sensitization and upconversion efficiency. This assumption is also supported by the experimental fact that the trend of the sensitization efficiency of **Lu-1** > **Lu-2** > **Lu-3** ~ **Lu-4** follows the lifetime order of Lu(III) complexes.

Table 2 Photophysical data in the sensitizer/BPEA upconversion systems (sensitizer = **Lu-1**, **Gd-1**, and **Pd-1**)[a]

	Lu-1	Gd-1	Pd-1
τ_0 [b] (μs)	2.4×10^3	104.7	414.9
τ [c] (μs)	26.4	16.8	12.3
K_{sv} (10^6 M^{-1})	1.8	0.1	1.3
Φ_{TTET} [d] (%)	99	84	98
Φ_{TTA} (%)	12.5	7.5	8.8
Φ_{UC} [e] (%)	12.4	6.3	8.6

[a] All data were measured in degassed toluene at room temperature. [b] Phosphorescence lifetime of sensitizers in the absence of BPEA. [c] Phosphorescence lifetime of sensitizers in the presence of BPEA (60 μM). [d] Calculated by the equation $\Phi_{TTET} = 1 - \tau/\tau_0$.[35]. [e] Using ZnTPP ($\Phi$ = 3.3%, in toluene) as a reference ([sensitizer] = 0.5 μM, λ_{ex} = 561 nm, 480 mW cm^{-2}).

$$\Phi_{UC} = \Phi_{ISC} \times \Phi_{TTET} \times \Phi_{TTA} \times \Phi_F. \quad (1)$$

In vitro cell imaging with up-converting nanomicelles (UC-NMs)

To demonstrate the potential application of Lu porphyrinates in TTA-UC based bioimaging, we prepared two kinds of upconverting nanoparticles with **Lu-1**/BPEA and **Lu-2**/BPEA pairs. Firstly, upconverting nanomicelles (UC-NMs) were prepared following the modified procedure reported by Meinardi and Beverina (Fig. 4a).[39] To circumvent the issues such as oxygen quenching and low water solubility,[40] polyethylene glycol 400 (PEG400) and 2,5-dimethylfuran (DMF) were chosen as the core solvent and $^1O_2$ scavenger, respectively.[41] The UC-NMs dispersed in water stably with no appreciable haze for a week. Fig. 4b and S36a† present the transmission electron microscopy (TEM) images of UC-NMs, which display spherical objects with a narrow diameter distribution peak at *ca.* 3 nm. The hydrodynamic diameter of the micelles is further analysed by dynamic light scattering (DLS). The hydrodynamic diameter of **Lu-1**/BPEA and **Lu-2**/BPEA UC-NMs was 5.3 ± 0.3 nm and 5.5 ± 0.3 nm, respectively (Fig. 4c and S39†). The hydrodynamic diameter is greater than the diameter measured by TEM, suggesting that the chromophore EL chains are extended in water. The successful loading of both chromophores was confirmed by absorption spectral analysis. As shown in Fig. 4d, the UV-Vis spectrum of **Lu-1**/BPEA UC-NMs in water showed the characteristic absorption of BPEA, which is in the region of 400–500 nm with well-defined vibronic structures, and the weak Q bands of **Lu-1** centered at 554 and 590 nm. Upon excitation at 561 nm, besides the residual **Lu-1** phosphorescence at 730 nm, the typical fluorescence of BPEA with delayed lifetime was also observed. Again, the control experiment in the absence of **Lu-1** did not display the fluorescence of BPEA excited at 561 nm. With ZnTPP as a reference,[30] the UC quantum yield was found to be 1.3% and 1.1% for **Lu-1**/BPEA and **Lu-2**/BPEA, respectively (480 mW cm^{-2}), suggesting an effective TTA-UC process in nanomicelles.

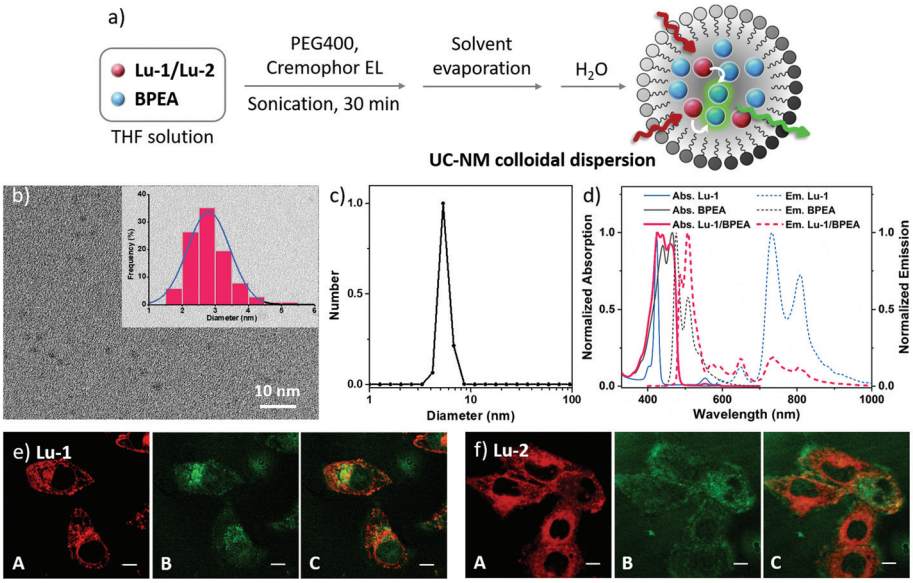

Fig. 4 (a) Illustration of the preparation scheme of UC-NMs, and the sketch of the TTA-UC process in a single UC-NM. (b) Transmission electron microscopy (TEM) image and (c) dynamic light scattering (DLS) of **Lu-1**/BPEA loaded UC-NM. (d) Normalized absorption and emission spectra of **Lu-1**/BPEA loaded UC-NM in water under an ambient atmosphere (λ_{ex} = 561 nm, 480 mW cm^{-2}). (e and f) Confocal fluorescence image of living HeLa cells with UC nanoparticles by 455–525 nm channel under laser excitation at (A) 405 nm (red, prompt fluorescence); (B) 543 nm (green, upconverted fluorescence); and (C) merged images of (A) and (B). Rows e and f: image of UC-NMs (incubated for 15 min) loaded with (e) **Lu-1**/BPEA and (f) **Lu-2**/BPEA (presented with fake color; scale bar presents 20 μm).

Further application of UC-NMs in bioimaging was demonstrated using a fluorescence confocal microscope. HeLa cells were incubated with UC-NMs for 15 min, and cyan fluorescence was observed with 455–525 nm channels for **Lu-1**/BPEA and **Lu-2**/BPEA UC-NMs in the cytoplasm region upon excitation at either 405 or 543 nm (Fig. 4e and f). Two signals can be roughly merged (Fig. 4e and f column C), indicating that the UC luminescence at 455–525 nm originated from the TTA-UCNMs. To exclude the possible artefacts, a negative control experiment was conducted using nanomicelles loaded with BPEA only (no sensitizers) (Fig. S43a†). Upon irradiation at 405 nm, strong luminescence was observed by the same channels, which was ascribed to the prompt fluorescence of BPEA. However, under irradiation of 561 nm, fluorescence was too weak to be detected. The above results clearly proved the upconversion imaging potential of TTA-UCNMs with Lu(III) porphyrinates as TTA-UC sensitizers, despite that the UC luminescence showed a limited signal-to-noise ratio (Fig. 4e and f, column B) and could not be completely overlapped with conventional fluorescence signals. We ascribe it to the instability of the nanomicelles, which resulted in the leakage of fluorescence and the permeation of oxygen.

In vitro cell imaging with up-converting mesoporous silica nanoparticles (UC-MSNs)

Considering the relatively low cytotoxicity and high stability of silica-based materials, we also prepared up-converting nanocapsules with mesoporous silica nanoparticles (MSNs). MSNs were prepared by following modification procedures described in the literature.[42] The TTA-UC chromophore pair in methyl oleate oil, which can efficiently prevent oxygen quenching, was then infused into mesoporous silica nanoparticles (UC-MSNs, Fig. 5a).[42] The TEM images indicated that the UC-MSN consists of uniform ellipsoidal nanoparticles with major/minor axis lengths of roughly 96/56 nm and 86/55 nm, for **Lu-1**/BPEA and **Lu-2**/BPEA UC-MSNs, respectively (Fig. 5b and S37–38†). At higher magnification, well-defined channels can also be identified both in the bright and dark field images (Fig. 5c), with a pore diameter estimated to be *ca.* 3 nm. Black and white dots were observed to be implanted in the MSNs in the bright and dark fields, respectively, which exhibit a stripe pattern filling the pore structure (Fig. 5c and S38b†). This should be the embedded chromophore pairs. As measured by the DLS technique, two groups of particles with average hydrodynamic diameters around (209 ± 4) and (438 ± 3) nm are observed with either UC-MSNs (Fig. 5d), which confirmed the nanorod morphology of UC-MSNs, and is in good agreement with the TEM result. As expected, UC-MSNs displayed upconversion emission similar to the UC-NMs in aqueous media upon excitation with a 561 nm laser (Fig. 5e), with UC quantum yields as 2.4% and 2.1% for **Lu-1**/BPEA and **Lu-2**/BPEA, respectively (480 mW cm^{-2}). Compared with the corresponding UC-NMs, the Φ_{UC}s doubled for up-converting mesoporous silica nanoparticles, and were comparable to previously reported water-soluble upconversion materials, including rare-earth UC nanophosphors and TTA-UC nanoparticles sensitized by d-block metal complexes.[43] Therefore, we assumed that with better prepared nanoparticles, Lu(III) porphyrinates/BPEA can achieve a higher TTA-UC efficiency in aqueous solution.

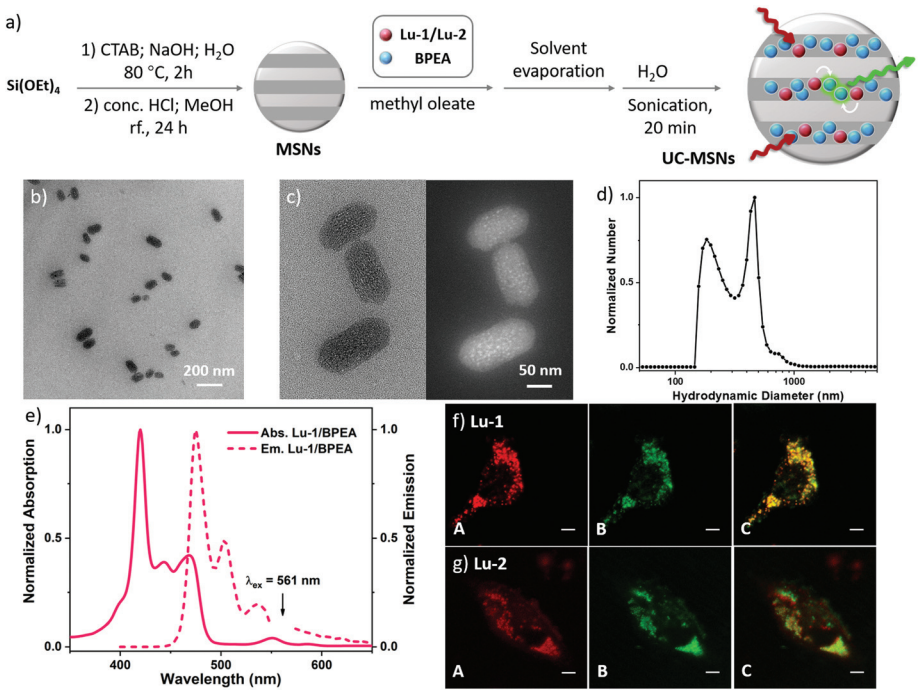

Fig. 5 (a) Illustration of the preparation scheme of UC-MSNs, and the sketch of the TTA-UC process in a single UC-MSN. (b) Transmission electron microscopy (TEM) image at 25k× magnification, (c) bright field (left) and dark field (right) TEM image at 60k× magnification, and (d) dynamic light scattering (DLS) of **Lu-1**/BPEA loaded UC-MSN. (e) Normalized absorption and emission spectra of **Lu-1**/BPEA loaded UC-MSN in water under an ambient atmosphere (λ_{ex} = 561 nm, 480 mW cm^{-2}). (f and g) Confocal fluorescence images of living HeLa cells with UC nanoparticles by a 455–525 nm channel under laser excitation at (A) 405 nm (red, prompt fluorescence); (B) 543 nm (green, upconverted fluorescence); and (C) merged images of (A) and (B). Rows f and g: images of UC-MSNs (incubated for 15 min) loaded with (f) **Lu-1**/BPEA and (g) **Lu-2**/BPEA (Presented with fake color; scale bar presents 20 μm).

Living cell imaging experiments were also performed with UC-MSNs (Fig. 5f and g). High-contrast UC fluorescence images (Fig. 5f and g, column B) were recorded. Furthermore, the UC luminescence signal at 455–525 nm well merged with the conventional fluorescence signal (Fig. 5f and g, column C), which probably results from the higher structural stability of silica nanoparticles than micelles. The results suggest the capability of **Lu-1** or **Lu-2** as a TTA sensitizer for potential application in living cell imaging.

Conclusions

In conclusion, we synthesized Lu(III) complexes of porphyrinoids as sensitizers in TTA upconversion. β-Lactonization of porphyrinic ligands lowers both singlet and triplet states, offering a way to tune the excitation and emission wavelength. The **Lu-1**/BPEA system shows a much higher TTA upconversion efficiency of 12.4% compared with Gd(III), Pd(II) and Zn(II) analogues, which is probably attributed to its extraordinarily long triplet lifetime. Furthermore, we achieved UC fluorescence in aerated water by encapsulating upconverted chromophore pairs inside self-assembled nanomicelles and mesoporous silica nanoparticles, which enable living HeLa cell imaging. This work not only expands the repertoire of TTA photosensitizers, but also helps in extending the scope of lanthanide coordination complexes in upconversion bioimaging based on TTA.

Experimental section

General materials and methods

Unless otherwise stated, all the chemicals used in the synthesis are analytical pure and were used as received and the reactions were performed under an inert atmosphere of nitrogen. ^{1}H NMR spectra were recorded on a 400 MHz Bruker spectrometer (TMS as the standard of the chemical shifts). ^{13}C and ^{19}F NMR spectra were recorded on a 500 MHz Bruker spectrometer. IR spectra were recorded with a PerkinElmer Spectrum Spotlight 200 FT-IR microscope. ESI mass spectra were recorded with a Bruker APEX IV FTICR mass spectrometer. The size and morphology of upconverting nanoparticles were determined with a JEOL JEM-2100F field-emission high resolution transmission electron microscope operated at 200 kV. UV/Vis absorption spectra were recorded with an Agilent 8453 UV/Vis spectrometer equipped with an Agilent 89090 A thermostat (±0.1 °C) at 25 °C. The emission spectra and phosphorescence lifetimes were recorded with an Edinburgh Analytical Instruments FLS920/FLS980 lifetime and steady-state spectrometer (a 450 W Xe lamp/microsecond flash

lamp, PMT R928 for visible emission spectra, a HAMAMATSU R5509-73 PMT with a C9940-02 cooler for NIR emission spectra and luminescence lifetimes). The time resolved emission spectra and lifetimes of delayed fluorescence were recorded with a Horiba Jobin Yvon DeltaFlex ultrafast lifetime spectrofluorometer. Confocal fluorescence microscopy of living cells was performed using a Nikon A1R-si laser scanning confocal microscope (Japan) equipped with 405 and 543 nm lasers. For optical measurements in liquid solution, anhydrous toluene was distilled.

Synthesis of compounds Lu-1–4 and Gd-1

The syntheses followed a similar procedure as described in the literature.[29] Free base porphyrinoid ligands (**1–4**) (50 mg, 0.05 mmol) and Ln(III) 2,4-pentanedionate hydrate ($Ln(acac)_3{\cdot}6H_2O$, 0.25 mmol) were dissolved in 1,2,4-trichlorobenzene (TCB, 8 mL) in a Schlenk tube, and was refluxed for 4 h under N_2. After cooling to room temperature, the reaction mixtures were transferred to a silica column, TCB was first eluted with petroleum ether, and then the unreacted free base ligand was eluted with CH_2Cl_2; the corresponding Ln(III) complexes were obtained by using CH_2Cl_2/MeOH (v/v = 5 : 1) as the eluent and used directly in the next step. The obtained Ln(III) complex ($acac^-$ as the ancillary ligand) and sodium(cyclopentadienyl)tris(dimethylphosphito)cobaltate(I) (NaL_{OMe}, *ca.* 2 equiv.) were dissolved in a mixed solvent of $CHCl_3/CH_3OH$ (v/v = 3 : 1, 5 mL) and was heated at reflux for 3 h. After cooling to room temperature, the reaction mixtures were transferred to a silica column, and the product was obtained by using ethyl acetate/petroleum ether (v/v = 15 : 1) as the eluent.

Complex Lu-1. Yield: 67 mg (82%, calculated on the basis of free base porphyrin ligand); ^{1}H NMR (400 MHz, $CDCl_3$): δ 8.80 (s, 8H), 4.13 (s, 5H), 2.32 (dd, J = 7.0, 3.6 Hz, 18H); ^{13}C NMR (126 MHz, $CDCl_3$) δ 151.16, 131.41, 106.02, 88.23, 50.50, 29.86; ^{19}F NMR (377 MHz, $CDCl_3$) δ −135.06 (4F), −137.41(4F), −153.08(4F), −161.97(4F), −162.96(4F); HRMS(ESI$^+$) m/z $[M + H]^+$: calculated for $C_{55}H_{32}CoF_{20}LuN_4O_9P_3$ 1598.98010, found 1598.98138; IR (cm^{-1}): 617, 712, 735, 764, 800, 843, 935, 9567, 987, 1011, 1045, 1076, 1120, 1161, 1178, 1261, 1333, 1377, 1485, 1518, 1633, 1649, 1728, 2850, 2925, 2945, 3388.

Complex Lu-2. Yield: 65 mg (80%, calculated on the basis of free base porpholactone ligand); ^{1}H NMR (400 MHz, $CDCl_3$): δ 8.62 (d, J = 4.7 Hz, 1H), 8.58 (t, J = 5.3 Hz, 2H), 8.54 (d, J = 4.7 Hz, 1H), 8.50 (dd, J = 8.7, 4.6 Hz, 2H), 4.27 (s, 5H), 2.52 (dd, J = 7.1, 3.6 Hz, 18H); ^{13}C NMR (126 MHz, $CDCl_3$) δ 166.09, 155.74, 152.88, 152.57, 152.06, 151.72, 149.18, 148.99, 133.62, 131.77, 130.52, 129.98, 128.83, 127.38, 112.13, 88.60, 77.41, 77.16, 76.91, 50.73, 32.08, 29.94, 29.86, 29.82, 29.52, 29.48, 27.37, 22.85, 14.27; ^{19}F NMR (377 MHz, $CDCl_3$) δ −135.29 (2F), −135.51 (1F), −137.61 (3F), −138.72 (1F), −139.53 (1F), −152.18 (2F), −152.43 (1F), −152.89 (1F), −161.31 (3F), −162.02 (1F), −162.35 (3F), −162.89 (1F); HRMS(ESI$^+$) m/z $[M + H]^+$: calculated for $C_{54}H_{30}CoF_{20}LuN_4O_{11}P_3$ 1616.95428, found 1616.95545; IR (cm^{-1}): 733, 762, 800, 847, 868, 930, 943, 958, 984, 1005, 1043, 1070, 1120, 1178, 1219, 1255, 1277, 1230, 1319, 1334, 1344, 1358, 1377, 1442, 1487, 1518, 1653, 1739, 1768 (C═O), 2951, 3118.

Complex Lu-3. Yield: 62 mg (76%, calculated on the basis of free base *cis*-porphodilactone ligand); ^{1}H NMR (400 MHz, $CDCl_3$): δ 8.42 (s, 2H), 8.26 (s, 2H), 4.42 (s, 5H), 2.72 (dd, J = 7.2, 3.7 Hz, 18H); ^{13}C NMR (126 MHz, $CDCl_3$) δ 165.17, 157.37, 153.78, 149.32, 133.14, 128.95, 128.59, 124.29, 111.59, 88.95, 68.32, 51.01, 38.90, 32.09, 30.53, 29.86, 29.52, 29.09, 23.91, 23.14, 22.85, 14.28, 11.12; ^{19}F NMR (471 MHz, $CDCl_3$) δ −135.55 (2F), −137.77 (2F), −138.97 (2F), −139.79 (2F), −151.42 (2F), −152.27 (2F), −160.69 (2F), −161.55 (2F), −161.79 (2F), −162.48 (2F); HRMS(ESI$^+$) m/z $[M + H]^+$: calculated for $C_{53}H_{28}CoF_{20}LuN_4O_{13}P_3$ 1634.92845, found 1634.92959; IR (cm^{-1}): 669, 704, 739, 764, 781, 845, 866, 877, 931, 951, 982, 1011, 1045, 1068, 1113, 1176, 1221, 1277, 1321, 1356, 1381, 1398, 1439, 1481, 1496, 1520, 1554, 1585, 1633, 1653, 1766 (C═O), 2846, 2910, 2951, 3120.

Complex Lu-4. Yield: 56 mg (69%, calculated on the basis of free base *trans*-porphodilactone ligand); ^{1}H NMR (400 MHz, $CDCl_3$): δ 8.52 (s, 4H), 4.35 (s, 5H), 2.65 (dd, J = 7.2, 3.7 Hz, 18H); ^{13}C NMR (126 MHz, $CDCl_3$) δ 165.17, 165.16, 152.92, 152.81, 151.04, 131.18, 130.79, 127.38, 92.65, 88.89, 50.93, 29.85; ^{19}F NMR (471 MHz, $CDCl_3$) −135.53 (2F), −137.64 (2F), −138.71 (2F), −139.78 (2F), −151.43 (2F), −152.19 (2F), −160.79 (2F), −161.60 (2F), −161.88 (2F), −162.52 (2F); δ HRMS(ESI$^+$) m/z $[M + H]^+$: calculated for $C_{53}H_{28}CoF_{20}LuN_4O_{13}P_3$ 1634.92845, found 1634.92719; IR (cm^{-1}): 621, 638, 677, 704, 735, 762, 783, 849, 868, 922, 945, 984, 1003, 1041, 1066, 1111, 1147, 1180, 1227, 1273, 1317, 1336, 1361, 1394, 1442, 1495, 1518, 1535, 1655, 1759 (C═O), 2850, 2951, 2991, 3122.

Complex Gd-1. Yield: 63 mg (78%, calculated on the basis of free base porphyrin ligand).

Synthesis of compound Pd-1

The synthesis followed a similar procedure described in the literature.[36] Yield: 78%.

Synthesis of compound Zn-1

The synthesis followed a similar procedure described in the literature.[44] Yield: 90%.

Synthesis of TTA-upconverting nanoparticles

Synthesis of TTA-upconverting nanomicelles (UCNMs). The synthesis followed a similar procedure described in the literature.[38] Cremophor EL (75 mg) and polyethylene glycol 400 (PEG400, 15 mg) were added to a tetrahydrofuran (THF) solution (1 mL) of sensitizer (**Lu-1** or **Lu-2**, 200 μM) and BPEA (3500 μM). The mixture was ultrasonicated for 30 min. All volatiles were evaporated and the oily residue was taken up with deionized water (5 mL) to give a UC-NM stable dispersion. The dispersion was stored in the dark at 4 °C for further experiments.

Synthesis of mesoporous silica nanoparticles (MSNs). The synthesis followed a similar procedure described in the literature.[42] Cetyl trimethylammonium bromide (CTAB, 2.0 g) was dissolved in 1000 mL of deionized water. Sodium hydroxide aqueous solution (2.0 M, 7.0 mL) was then added to the CTAB

solution. After the mixture was heated to 80 °C, tetraethoxysilane (TEOS, 10.0 mL) was added dropwise to the mixture under vigorous stirring. The mixture was allowed to react for another 2 h to give a white precipitate. This solid crude white product was filtered, washed with water and methanol, and dried in air to yield the as-synthesized mesoporous silica nanoparticles (MSN). 1.5 g of as-synthesized MSN was added to a methanolic solution (160 mL methanol) of HCl (37.4%, 9.0 mL). The mixture was refluxed for 24 h to remove the surfactant template (CTAB). The resulting material was filtered and extensively washed with water and methanol followed by vacuum drying for 24 h at room temperature for further experiments.

Synthesis of TTA-upconverting mesoporous silica nanoparticles (UC-MSNs). The synthesis followed a similar procedure described in the literature.[42] MSNs (50.0 mg) were dispersed in a 25 mL round-bottomed flask that contained the sensitizer (**Lu-1** or **Lu-2**, 2 μmol), BPEA (7.0 mg), and methyl oleate (150 mg) in THF (10 mL). The mixture was stirred in a dark fumehood at room temperature to evaporate the organic solvent (*ca.* 12 h), and then ultrasonicated in 10 mL phosphate-buffered saline (PBS) for 20 min followed by 5 min of low-speed centrifugation (1000 rpm min^{-1}) to remove the excess reactants. The UC-MSNs were collected from the precipitate and dried at 40 °C for 24 h under vacuum and stored in the dark for further experiments.

Phosphorescence and upconverted quantum yields determination

Unless otherwise stated, optical measurements in liquid solution were performed by degassing by five freeze–pump–thaw cycles. Phosphorescence quantum yields were measured with ZnTPP (Φ_F = 3.3% in toluene)[30] as the standard according to the equation: $\Phi_{sam} = \Phi_{std} \times (A_{std}/A_{sam}) \times (I_{sam}/I_{sam}) \times (n_{sam}^2/n_{sam}^2)$, where Φ_{sam}, A_{sam}, I_{sam} and n_{sam} represent the quantum yield, absorbance, integrated photoluminescence intensity and refractive index of the samples. Symbols with 'std' stand for the corresponding parameter for the standard. Lasers (continuous laser, 561 nm, 639 nm and 659 nm) were used as the excitation source for the upconversion. The power of the laser beam was measured with a laser power meter. The upconversion quantum yields were measured with ZnTPP (λ_{ex} = 561 nm) or methylene blue (λ_{ex} = 639 or 659 nm, Φ_F = 3.0% in MeOH)[45] as the standard according to the equation:

$$\Phi_{sam} = 2\Phi_{std} \times (A_{std}/A_{sam}) \times (I_{sam}/I_{sam}) \times (n_{sam}^2/n_{sam}^2).$$

Triplet–triplet energy transfer efficiency measurement

Φ_{TTET} was calculated according to the equation: $\Phi_{TTET} = 1 - \tau/\tau_0$,[35] where τ_0 and τ represent the phosphorescence lifetime of the sensitizer in the absence and in the presence of an annihilator, respectively.

Cell culture

HeLa cells were cultured in Dulbecco's modified Eagle's medium (DMEM, Gibco) supplemented with 10% fetal bovine serum (FBS), 1% penicillin and streptomycin. HeLa cells were grown at 37 °C under a humidified atmosphere containing 5% CO_2.

Cell imaging

Cells were placed on sterile glass coverslips in cell culture dishes containing complete media and allowed to grow to about 80% confluence. Nanomicelles (UC-MNs, 1 : 20 of the initial dispersion) or mesoporous silica nanoparticles (UC-MSNs, 200 μg mL^{-1} dissolved in PBS) were added. After 15 min for UC-MNs and 4 h for UC-MSNs, confocal fluorescence microscopy of living cells was performed (a 543 nm laser was used for upconversion imaging due to the lack of a 561 nm laser.).

Conflicts of interest

There are no conflicts to declare.

Acknowledgements

We acknowledge the financial support from the National Key Basic Research Support Foundation of China (2015CB856301) and the National Scientific Foundation of China (Grant No. 21778002, 21621061 and 21571007). M. Chen and Y. Guan are gratefully thanked for their help with photophysical measurements and cell imaging.

Notes and references

1 T. N. Singh-Rachford and F. N. Castellano, *Coord. Chem. Rev.*, 2010, **254**, 2560.
2 J. Zhou, Q. Liu, W. Feng, Y. Sun and F. Y. Li, *Chem. Rev.*, 2015, **115**, 395.
3 X. Guo, Y. Liu, Q. Chen, D. Zhao and Y. Ma, *Adv. Opt. Mater.*, 2018, **6**, 1700981.
4 N. Yanai and N. Kimizuka, *Acc. Chem. Res.*, 2017, **50**, 2487.
5 X. J. Zhu, Q. Q. Su, W. Feng and F. Y. Li, *Chem. Soc. Rev.*, 2017, **46**, 1025.
6 Q. Q. Dou, L. Jiang, D. Kai, C. Owh and X. J. Loh, *Drug Discovery Today*, 2017, **22**, 1400.
7 N. J. Turro, V. Ramamurthy and J. C. Scaiano, *Principles of Molecular Photochemistry: An Introduction*, University Science Books, Sausalito, CA, 2009.
8 M. Montalti, A. Credi, L. Prodi and M. T. Gandolfi, *Handbook of Photochemistry*, CRC Press, Taylor & Francis Group, Boca Raton, FL, 3 edn, 2006.
9 J. Z. Zhao, W. H. Wu, J. F. Sun and S. Guo, *Chem. Soc. Rev.*, 2013, **42**, 5323.
10 Z. Xun, Y. Zeng, J. Chen, T. Yu, X. Zhang, G. Yang and Y. Li, *Chem. – Eur. J.*, 2016, **22**, 8654.
11 S. V. Eliseeva and J. C. Bunzli, *Chem. Soc. Rev.*, 2010, **39**, 189.
12 K. Binnemans, *Chem. Rev.*, 2009, **109**, 4283.

13 J. C. G. Bünzli, *Chem. Rev.*, 2010, **110**, 2729.
14 Selected examples: (*a*) J. L. Sessler, W. C. Dow, D. O'Connor, A. Harriman, G. Hemmi, T. D. Mody, R. A. Miller, F. Qing, S. Springs, K. Woodburn and S. W. Young, *J. Alloys Compd.*, 1997, **249**, 146; (*b*) Y. Zhou, C. F. Chan, D. W. J. Kwong, G. L. Law, S. Cobb, W. K. Wong and K. L. Wong, *Chem. Commun.*, 2017, **53**, 557; (*c*) J. X. Zhang, H. Li, C. F. Chan, R. Lan, W. L. Chan, G. L. Law, W. K. Wong and K. L. Wong, *Chem. Commun.*, 2012, **48**, 9646; (*d*) T. Zhang, R. Lan, C. F. Chan, G. L. Law, W. K. Wong and K. L. Wong, *Proc. Natl. Acad. Sci. U. S. A.*, 2014, **111**, E5492.
15 V. Bulach, F. Sguerra and M. W. Hosseini, *Coord. Chem. Rev.*, 2012, **256**, 1468.
16 M. Gouterman, R. J. Hall, G.-E. Khalil, P. C. Martin, E. G. Shankland and R. L. Cerny, *J. Am. Chem. Soc.*, 1989, **111**, 3702.
17 J. R. McCarthy, H. A. Jenkins and C. Brückner, *Org. Lett.*, 2003, **5**, 19.
18 B. Kalota and M. Tsvirko, *Chem. Phys. Lett.*, 2015, **634**, 188.
19 X. S. Ke, Y. Ning, J. Tang, J. Y. Hu, H. Y. Yin, G. X. Wang, Z. S. Yang, J. Jie, K. Liu, Z. S. Meng, Z. Zhang, H. Su, C. Shu and J. L. Zhang, *Chem. – Eur. J.*, 2016, **22**, 9676.
20 Z. S. Yang, Y. Ning and J. L. Zhang, *J. Chin. Soc. Rare Earths*, 2016, **34**, 764.
21 S. Tobita, M. Arakawa and I. Tanaka, *J. Phys. Chem.*, 1984, **88**, 2697.
22 S. Tobita, M. Arakawa and I. Tanaka, *J. Phys. Chem.*, 1985, **89**, 5649.
23 X. S. Ke, B. Y. Yang, X. Cheng, S. L. Chan and J. L. Zhang, *Chem. – Eur. J.*, 2014, **20**, 4324.
24 Y. Y. Ning, X. S. Ke, J. Y. Hu, Y. W. Liu, F. Ma, H. L. Sun and J. L. Zhang, *Inorg. Chem.*, 2017, **56**, 1897.
25 J. Y. Hu, Y. Ning, Y. S. Meng, J. Zhang, Z. Y. Wu, S. Gao and J. L. Zhang, *Chem. Sci.*, 2017, **8**, 2702.
26 Y. Y. Ning, Y. W. Liu, Y. S. Meng and J. L. Zhang, *Inorg. Chem.*, 2018, **57**, 1332.
27 Y. Y. Ning, J. Tang, Y. W. Liu, J. Jing, Y. S. Sun and J. L. Zhang, *Chem. Sci.*, 2018, **9**, 3742.
28 W. Kläui, M. Berghahn, G. Rheinwald and H. R. Lang, *Angew. Chem., Int. Ed.*, 2000, **39**, 2464.
29 F. Gao, M. X. Yao, Y. Y. Li, Y. Z. Li, Y. Song and J. L. Zuo, *Inorg. Chem.*, 2013, **52**, 6407.
30 M. Pineiro, A. L. Carvalho, M. M. Pereira, A. M. d'A. Rocha Gonsalves, L. G. Arnaut and S. J. Formosinho, *Chem. – Eur. J.*, 1998, **4**, 2299.
31 S. M. Borisov, G. Nuss and I. Klimant, *Anal. Chem.*, 2008, **80**, 9435.
32 P. J. Spellane, M. Gouterman, A. Antipas, S. Kim and Y. C. Liu, *Inorg. Chem.*, 1980, **19**, 386.
33 A. Monguzzi, R. Tubino and F. Meinardi, *J. Phys. Chem. A*, 2009, **113**, 1171.
34 T. N. Singh-Rachford and F. N. Castellano, *J. Phys. Chem. A*, 2008, **112**, 3550.
35 T. W. Schmidt and F. N. Castellano, *J. Phys. Chem. Lett.*, 2014, **5**, 4062.
36 X. S. Ke, H. M. Zhao, X. R. Zou, Y. Y. Ning, X. Cheng, H. M. Su and J. L. Zhang, *J. Am. Chem. Soc.*, 2015, **137**, 10745.
37 A. Demeter, *J. Phys. Chem. A*, 2014, **118**, 9985.
38 G. E. Khalil, E. K. Thompson, M. Gouterman, J. B. Callis, L. R. Dalton, N. J. Turro and S. Jockusch, *Chem. Phys. Lett.*, 2007, **435**, 45.
39 S. Mattiello, A. Monguzzi, J. Pedrini, M. Sassi, C. Villa, Y. Torrente, R. Marotta, F. Meinardi and L. Beverina, *Adv. Funct. Mater.*, 2016, **26**, 8447.
40 S. Baluschev, K. Katta, Y. Avlasevich and K. Landfester, *Mater. Horiz.*, 2016, **3**, 478.
41 C. Mongin, J. H. Golden and F. N. Castellano, *ACS Appl. Mater. Interfaces*, 2016, **8**, 24038.
42 L. Huang, Y. Zhao, H. Zhang, K. Huang, J. Yang and G. Han, *Angew. Chem., Int. Ed.*, 2017, **56**, 14400.
43 Q. Liu, T. S. Yang, W. Feng and F. Y. Li, *J. Am. Chem. Soc.*, 2012, **134**, 5390.
44 Y. Yu, H. Lv, X. Ke, B. Yang and J. L. Zhang, *Adv. Synth. Catal.*, 2012, **354**, 3509.
45 J. Olmsted, *J. Phys. Chem.*, 1979, **83**, 2581.